Supplementary Information for:

Formic acid – methanol complexation vs esterification: Elusive pre-reactive species identified by vibrational spectroscopy

Sophie M. Schweer, Maxim Gawrilow, Arman Nejad,[‡] and Martin A. Suhm*

Institute of Physical Chemistry, University of Goettingen, Tammannstr. 6, 37077 Goettingen, Germany.
[‡] *Current address: Physical and Theoretical Chemistry Laboratory, University of Oxford, South Parks Road, Oxford OX1 3QZ, UK.*
E-mail: msuhm@gwdg.de

Contents

S1 Auxiliary data for Sec. 3 "Results and discussion"

S1.1 Sec. 3.1 "Computational thermodynamics of ester formation"

S1.1.1 Details on quantum chemical calculations

Structure optimisation and frequency calculations on DFT level were performed with B3LYP and PBE0 functionals, def2-QZVPP basis set, Grimme's dispersion correction with Becke-Johnson damping and three-body-terms D3(BJ,abc)(*1*, *2*), integration grid m5, main isotope masses, SCF convergence of $1 \cdot 10^{-9}\,E_\mathrm{h}$ and a structure convergence of $1 \cdot 10^{-6}\,E_\mathrm{h}$. For speedup, resolution of the identity for Coulomb and Exchange integrals RIJK was used(*3*). Turbomole was employed, using the default values for all remaining parameters(*4*). Structure optimisation on CCSD(T) level with explicit correlation (F12A) was performed with cc-pVDZ-F12 basis set, density fitting (DF) and frozen core(*5*, *6*) using Molpro(*7*–*9*). Except for the SCF convergence ($1 \cdot 10^{-9}\,E_\mathrm{h}$) all parameters were kept at their default values. Single point CCSD(T) energies with explicit correlation (F12*)(*10*–*12*) were calculated with cc-pVTZ-F12 basis set, resolution of identity for Coulomb and Exchange integrals (RIJK)(*3*), frozen core and SCF convergence $1 \cdot 10^{-9}\,E_\mathrm{h}$ using Turbomole(*4*), all other parameters were kept at their default values. In order to find optimal structures of ester-water, methanol-formic acid and CO_2 – H_2O – CH_4 an automated search using CREST version 2.7.1(*13*) at GFN2-xTB level(*14*–*16*) was performed, followed with a preoptimisation on RIJ-b97-3c/def2-mTZVP level using Turbomole(*4*). In this part, abbreviations will be used to denote the quantum chemical methods employed (Tab. S1). All calculations were performed without BSSE correction.

Tab. S1 Abbreviations of quantum chemical methods used in this section.

Abbreviation	Description
B3	structure optimisation RIJK-B3LYP-D3(BJ,abc)/def2-QZVPP(*1*–*3*)
P0	structure optimisation RIJK-PBE0-D3(BJ,abc)/def2-QZVPP(*1*–*3*)
CC_{opt}	structure optimisation DF-CCSD(T)-F12A/cc-pVDZ-F12(*5*, *6*)
CC_{sp}	single point energy RIJK-CCSD(F12*)(T*)/cc-pVTZ-F12(*3*, *10*–*12*)
$MP2_{sp}$	single point energy RIJK-MP2-F12/cc-pVTZ-F12
ZPE_{xy}	zero point energy

S1.1.2 Guinness molecule for $C_2H_6O_3$ sum formula

Tab. S2 Absolute CCSD(T) energies for structures (see Fig. S1) optimised at different levels of theory and their difference Δ. The error for calculating CCSD(T) single point energies on top of B3LYP instead of CCSD(T) optimised structures is at most 0.4 kJ mol^{-1}. For MP2$_{sp}$, this error amounts to 0.5 kJ mol^{-1}.

	CC_{sp}//B3 /E_h	CC_{sp}//CC_{opt} /E_h	Δ/kJ mol^{-1}
EW_CO_F	−305.207 898	−305.208 059	0.4
EW_CO_M	−305.208 877	−305.208 999	0.3
MF_bridge	−305.209 753	−305.209 739	<0.1
MF_open	−305.207 110	−305.207 109	<0.1
H_2O (W)	−76.371 418	−76.371 424	<0.1
MeOH (M)	−115.604 521	−115.604 520	<0.1
HCOOH (F)	−189.587 315	−189.587 308	<0.1
$HCOOCH_3$ (E)	−228.827 480	−228.827 558	0.2
CH_4	−40.455 201	−40.455 201	<0.1
CO_2	−188.409 578	−188.409 572	<0.1

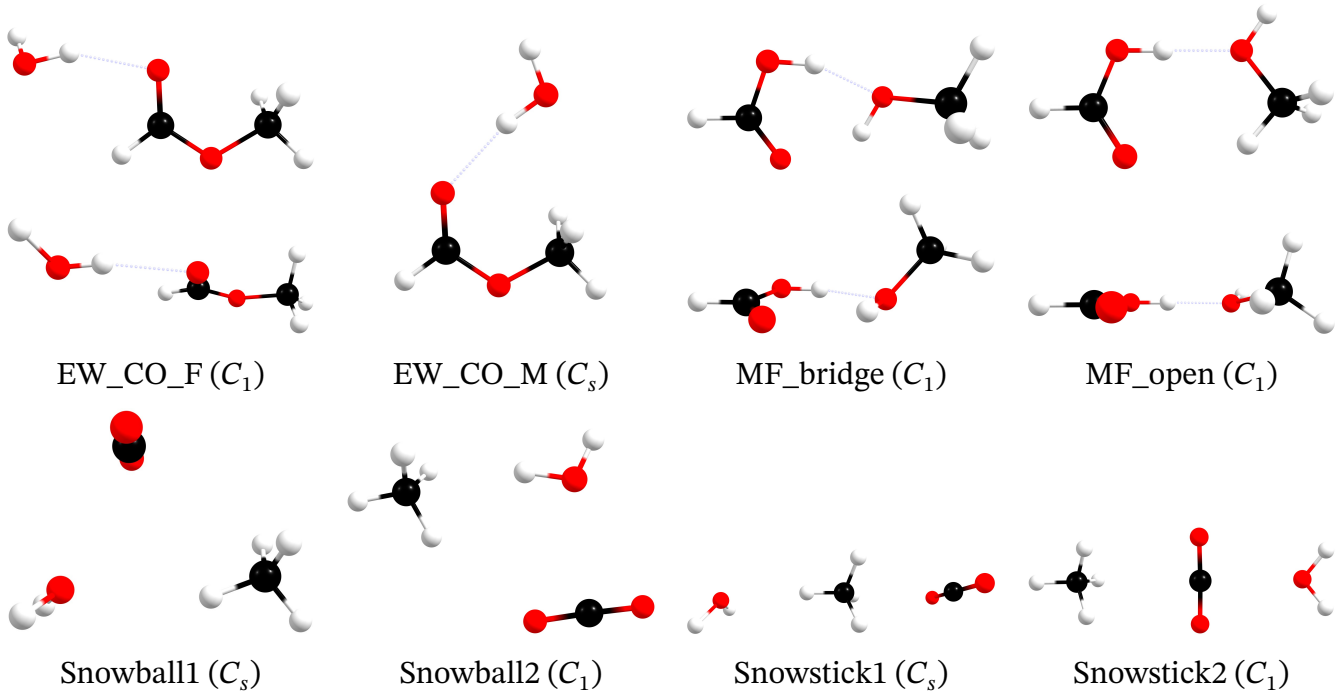

Fig. S1 Different stable arrangements of the sum formula $C_2H_6O_3$. (top row) The two most stable structures for complexes of formate ester with water (EW) and methanol with formic acid (MF). For EW, the water binds to the carbonyl oxygen (CO) and can point either to the formic acid (F) or methyl (M) side. For MF, the OH of methanol can either bind back to the formic acid (bridge) or point away from it (open). (bottom row) Four stable arrangements of CO_2, H_2O and CH_4, which all are approx. 100 kJ mol^{-1} more stable (including ZPE) than any of EW or MF (see Tab. S3).

Tab. S3 Relative harmonic ZPE-corrected energies at 0 K (ΔE_0, in kJ mol^{-1}) and standard Gibbs energies at 298 K ($\Delta_{298\,\mathrm{K}}G°$, in kJ mol^{-1}) of different arrangements for the sum formula $C_2H_6O_3$ (see Fig. S1). For CC, the non-electronic components (ZPE, enthalpy, entropy) are computed in the harmonic approximation with B3 on the B3 geometry. The ester-water complex is predicted to be more stable than the acid-alcohol one at CCSD(T) level, but both DFT functionals deviate qualitatively from the CCSD(T) result at 0 K. At infinite separation, all methods agree that ester and water are more stable. Although not achievable in our experiment, a hypothetical rearrangement to water, methane and CO_2 would release more than 100 kJ mol^{-1}.

	ΔE_0				$\Delta_{298\,\mathrm{K}}G°$			
	B3	P0	CC_{sp}//B3	CC_{sp}//CC_{opt}	B3	P0	CC_{sp}//B3	CC_{sp}//CC_{opt}
EW_CO_F	2.2	2.0	1.9	1.8	0.5	0.2	0.2	0.1
EW_CO_M	0	0	0	0	0	0	0	0
MF_bridge	−2.3	−4.9	2.1	2.5	0.8	−1.7	5.2	5.6
MF_open	2.8	1.5	7.1	7.4	3.8	2.2	8.1	8.4
Snowball1	−109.3	−99.2	−106.0	—	−129.8	−119.2	−123.9	—
Snowball2	−109.6	−99.6	−106.4	—	−129.2	−119.2	−123.9	—
Snowstick1	−108.8	−98.5	−105.5	—	−141.8	−133.9	−138.9	—
Snowstick2	−101.3	−91.6	−97.5	—	−136.1	−127.1	−130.9	—
Infinite separation								
H_2O + $HCOOCH_3$	19.2	19.2	18.4	18.5	−11.2	−11.5	−12.0	−11.9
MeOH + HCOOH	38.6	37.4	41.2	41.5	1.9	0.4	4.4	4.8
H_2O + CO_2 + CH_4	−98.0	−87.3	−94.2	−93.9	−157.9	−147.5	−154.1	−153.8

S1.2 Sec. 3.2 and 3.3 on "OH stretching signatures of complexes between methanol and formic acid"

S1.2.1 Details on quantum chemical calculations

Structure optimisation and frequency calculations for spectroscopic evalution on DFT level were performed with the B3LYP functional, def2-QZVP basis set, Grimme's dispersion correction with Becke-Johnson damping D3(BJ),(*1*, *2*) superfine integration grid, main isotope masses, with full optimisation (fopt=superfine). For dissociation energies, the PBE0 functional with D3(BJ) was used, additionally. Gaussian 16 (Rev. A.03) was employed, using the default values for all remaining parameters. The details for the anharmonic vibrational frequency calculations have been given in the main text. For sake of completeness, the keywords are listed below. Before calculating the anharmonic MP2 force fields and dipole derivatives ("freq=anharm") with Gaussian 16 (Rev. A.03), the geometries were optimised in a separate calculation using strict thresholds ("opt=verytight"). The CCSD(T)-F12a harmonic wavenumbers were calculated with Molpro version 2021.3 ("frequencies") following a geometry optimisation in Cartesian coordinates ("gthresh, optstep=6.d-5, optgrad=1.d-6, energy=1.d-10, zero=1.d-16", "optg, gaussian, grms=1.d-5, srms=1.d-5") using main isotope masses ("mass,iso") and enabling symmetry wherever available ("symmetry", "orient").

S1.2.2 Equilibrium geometries of methanol, formic acid, and their complexes

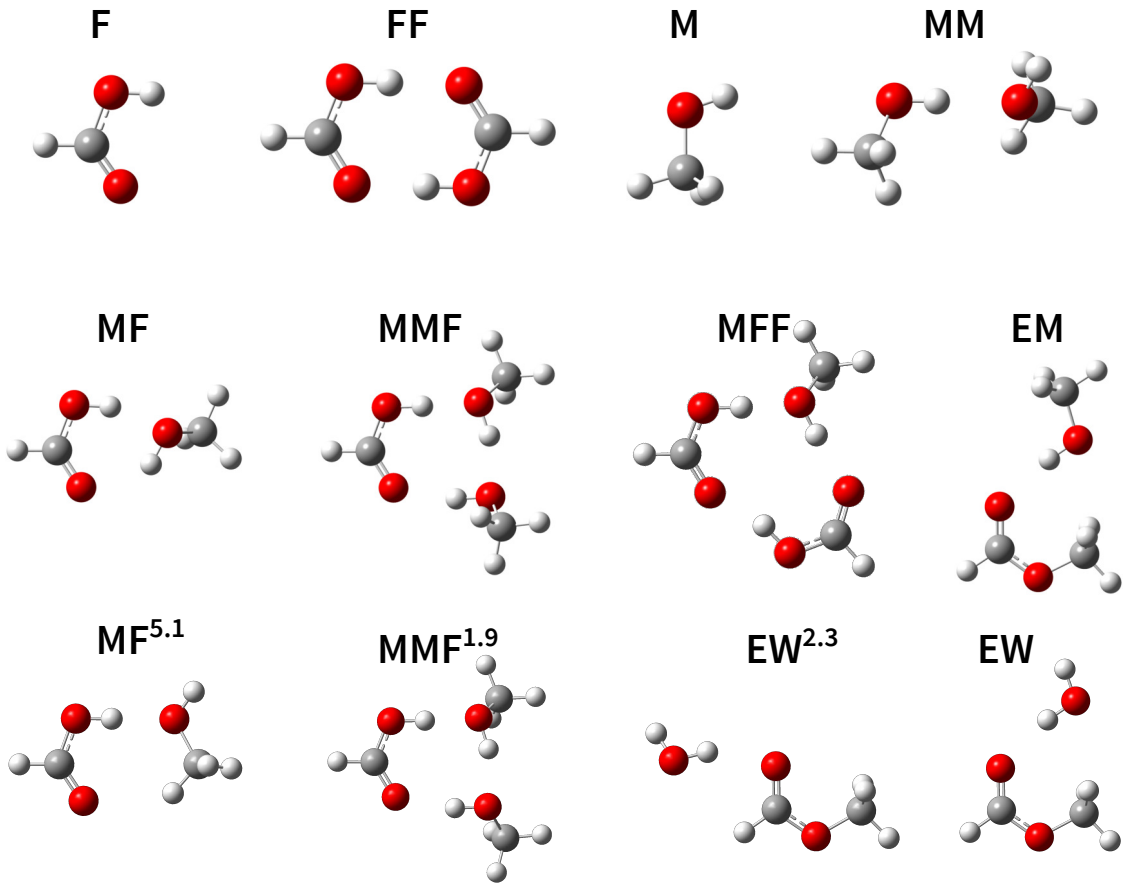

Fig. S2 Equilibrium geometries and their metastable isomers (up to 9 kJ/mol) of formic acid (F) and methanol (M) and their homodimers and selected mixed dimers and trimers optimised with Gaussian 16 at the B3LYP-D3(BJ)/def2-QZVP level. The methyl formate (E) complexes with methanol as well as water are also included. Vibrational spectroscopic properties and energies are reported in Tab. S4 (harmonic DFT) and S5 (post-HF VPT2).

S1.2.3 Vibrational spectroscopic properties

Tab. S4 Spectroscopic properties (harmonic OH stretching wavenumber ω_{OH}, downshift $-\Delta\omega_{OH}$ relative to the respective M and F monomer (M/F), infrared band strength S_ω, Raman differential cross section σ_{Raman} corrected for instrument properties and energies, relative conformational energy ΔE_0 and dissociation energies $D_{e/0}$ without and with zero point energy correction into the respective monomer structures) for different species optimised at the B3LYP-D3(BJ)/def2-QZVP level. Structures are shown in Figure S2. Some metastable isomers up to 9 kJ/mol are listed with their relative energy in kJ/mol as a superscript.

	ΔE_0	ω_{OH}	$-\Delta\omega_{OH}$ (M/F)		S_ω	σ_{Raman}	D_e	D_0
	kJ mol^{-1}	cm^{-1}	cm^{-1}		km mol^{-1}	10^{-35}m^{2}sr^{-1}	kJ mol^{-1}	kJ mol^{-1}
F	-	3727	-	-	60	6.6	-	-
FF	-	3156	-	571	2166	0	73.8	66.2
		3030	-	697	0	26.1		
M	-	3840	-	-	31	6.2	-	-
MM	-	3837	3	-	42	5.9	25.7	20.1
		3669	171	-	530	14.9		
MF	0	3656	184	71	317	6.1	49.2	41.2
		3233	607	494	830	16.1		
MF$^{5.1}$	5.1	3848	−8	−121	48	7.3	42.1	36.1
		3315	525	412	977	16.2		
MMF	0	3538	246	189	906	9.2	106.0	91.7
		3347	493	380	1003	13.4		
		2868	973	859	1699	24.1		
MMF$^{1.9}$	1.9	3541	299	186	902	9.3	103.9	89.8
		3366	474	361	919	12.0		
		2885	955	842	1685	23.7		
MFF	0	3475	366	253	1168	10.0	115.3	102.8
		3277	564	450	1214	16.7		
		2793	1048	934	1884	22.2		
EM	0	3710	130	-	453	13.1	47.3	40.0
EW	0	3886	-	-	94	4.9	46.8	37.0
		3695	-	-	322	12.0		
EW$^{2.3}$	2.3	3886	-	-	94	4.2	43.8	34.8
		3682	-	-	349	15.0		

Tab. S5 OH stretching wavenumbers and hydrogen bond-induced downshifts $-\Delta_{OH}$ (in cm^{-1}) calculated using the CCSD(T)-F12a/VDZ-F12//MP2/aVTZ hybrid force field. The VPT2 downshifts for the methanol - formic acid complexes are consistently larger than CCSD(T) harmonic shifts by 15-21%, suggesting the potential success of harmonic scaling approaches. Note, however, that the harmonic downshift deviation at CCSD(T) level is usually opposite to that at B3LYP level (Tab. S4), due to the excessive softness of OH bonds in this hybrid functional.

		ν(OH)		$-\Delta_{OH}$(M/F)	
		harm	VPT2	harm	VPT2
F		3759	3575		
M		3864	3691		
MF	OH_M	3709	3514	155	178
	OH_F	3351	3087[a]	407	488
MMF	OH_M	3636	3426	228	266
	OH_M	3480	3228	384	463
	OH_F	3054	–[b]	705	–
MFF	OH_M	3593	3369	271	322
	OH_F	3435	3182	324	393
	OH_F	3004	–[b]	754	–
EM		3760	3592	104	100

[a] Fermi triad at **3087**, 3133, and 3175 (fundamental bolded).

[b] Heavily perturbed by Fermi resonances.

Tab. S6 Selected DFT/def2-QZVP and CCSD(T)-F12a/VDZ-F12 dissociation energies (in kJ mol^{-1}) into monomer units with (ΔD_0) and without (ΔD_e) vibrational zero-point correction of some relevant complexes. Comparison to the coupled cluster approach shows the overbinding of the DFT values and the relative insignificance of anharmonic (VPT2) MP2-level corrections.

	B3LYP-D3(BJ)		PBE0-D3(BJ)		CCSD(T)-F12a		
	ΔD_e	$\Delta D_{0,h}$[a]	ΔD_e	$\Delta D_{0,h}$[a]	ΔD_e	$\Delta D_{0,h}$[a]	$\Delta D_{0,VPT2}$[b]
FF	73.8	66.2	75.9	68.9	67.7	59.3	59.9
MM	25.7	20.1	25.6	20.1			
MF	49.2	41.2	50.2	42.3	46.7	38.7	39.1
MMF	106.0	91.7	106.9	93.1	98.1	83.6	84.4
MFF	115.3	102.8	116.7	104.9	105.8	92.6	93.3
EM	47.2	40.0	46.8	39.8			

[a] Harmonic zero-point correction.

[b] Substituted hybrid force field approach using an MP2/aVTZ-level semi-diagonal quartic force field.

S1.2.4 Impact of CH deuteration on OH stretching wavenumbers

Tab. S7 Impact of CH deuteration on the OH stretching fundamentals (in cm^{-1}) of MF, MFF, and MMF at the harmonic B3LYP-D3(BJ)/def2-QZVP and CCSD(T)-F12a/VDZ-F12 level – abbreviated as "DFT" and "CC", respectively. The latter is augmented by MP2/aVTZ VPT2 corrections for the resonance-free fundamentals (substituted approach). The OH stretching wavenumber of the main isotopologue is reported together with the CH → CD isotope shift. The large isotope shift in MF results from a (predicted) strengthening of the OH_F Fermi resonance with the C=O stretching and F-centred OH bending combination level which energetically moves towards OH_F.

		DFT(harm)		CC(harm)		CC(VPT2)	
		ω_e	$\Delta\omega_e$	ω_e	$\Delta\omega_e$	$\tilde{\nu}$	$\Delta\tilde{\nu}$
MF	OH_M	3656.4	−0.3	3709.0	−0.2	3513.6	1.5
	OH_F	3233.4	−1.8	3351.3	−1.0	3087.0[a]	−38.6[b]
MMF	OH_M	3537.8	−0.7	3636.5	−0.5	3425.9	−0.4
	OH_M	3347.2	−1.5	3480.4	−0.8	3228.5	−2.0
	OH_F	2867.8	3.8	3054.0	4.4	–	–
MFF	OH_M	3474.7	−0.9	3593.5	−0.6	3369.3	0.5
	OH_F	3276.8	−1.5	3435.0	−0.7	3182.4	−2.8
	OH_F	2792.8	2.7	3004.4	9.5	–	–

[a] (CH) Fermi triad at **3087**, 3133, and *3175* (fundamental bolded, $\nu_{C=O} + \delta_{OH}$ italicised).

[b] (CD) Fermi triad at **3048**, 3102, and *3145* (fundamental bolded, $\nu_{C=O} + \delta_{OH}$ italicised); third state differs from *a*.

S1.2.5 Quantification of experimental abundance based on Beer's law

$$\frac{c}{\mathrm{cm}^3} = C \cdot \frac{\int A \mathrm{d}\tilde{\nu}}{\mathrm{cm}^{-1}} \cdot \left[\frac{S_\omega}{\mathrm{km\,mol}^{-1}}\right]^{-1} \quad \text{(S1)}$$

- c : estimated particle concentration of the compound
- $C = N_\mathrm{A}\mathrm{mol\,cm}/(10^5 d) \approx 10^{17}$ (for a slit jet with $d = 60\,\mathrm{cm}$)
- $\int A \mathrm{d}\tilde{\nu}$: area of the band of the investigated compound in the natural absorbance spectrum $A = \ln(\frac{I_0}{I}) \approx 2.3\,\lg(\frac{I_0}{I})$
- S_ω : predicted infrared band strength, here employing the double-harmonic approximation

Tab. S8 Quantification of average abundance based on integration of the absorbance signals with a numerical integration with a straight line via OriginLab[17]. For the chosen spectra, the corresponding figure number and trace are listed. For every monomer and cluster, the determined area $\lg(I_0/I)$ is listed with the $\tilde{\nu}_\mathrm{upper}$ and $\tilde{\nu}_\mathrm{lower}$ integration limit. The integral for F could not be determined for every spectrum because of its overlap with the MM band. The used infrared band strengths can be found in Tab. S4. Eq. S1 was used to estimate the abundance.

Figure	Structure	$\lg(I_0/I)$ / 10^{-3} cm^{-1}	$\tilde{\nu}_\mathrm{upper} - \tilde{\nu}_\mathrm{lower}$ / cm^{-1}	amount / cm^{-3}
2c+3c	M	2.7	3706−3671	2.0×10^{13}
	F	-	-	-
	MF	0.60	3533−3511	4.3×10^{11}
	MMF	0.69	3442−3422	1.8×10^{11}
	MFF	1.16	3386−3368	2.3×10^{11}
9c	M	1.53	3706−3671	1.2×10^{13}
	F	2.19	3589−3551	8.4×10^{12}
	MF	0.37	3533−3511	2.7×10^{11}
	MMF	0.23	3442−3422	5.9×10^{10}
	MFF	0.47	3386−3368	9.2×10^{10}
	EM	0.10	3597−3588	5.2×10^{10}
9d	M	1.53	3706−3671	1.2×10^{13}
	F	1.76	3589−3551	6.7×10^{12}
	MF	0.29	3533−3511	2.1×10^{11}
	MMF	0.13	3442−3422	3.3×10^{10}
	MFF	0.29	3386−3368	5.7×10^{10}
	EM	0.08	3597−3588	3.8×10^{10}
S3c	M	1.04	3706−3671	7.8×10^{12}
	F	4.15	3589−3551	1.6×10^{13}
	MF	0.55	3533−3511	4.0×10^{11}
	MMF	0.39	3442−3422	1.0×10^{11}
	MFF	2.27	3386−3368	4.5×10^{11}

S1.2.6 FTIR jet spectra from 2700 to 3800 cm^{-1}

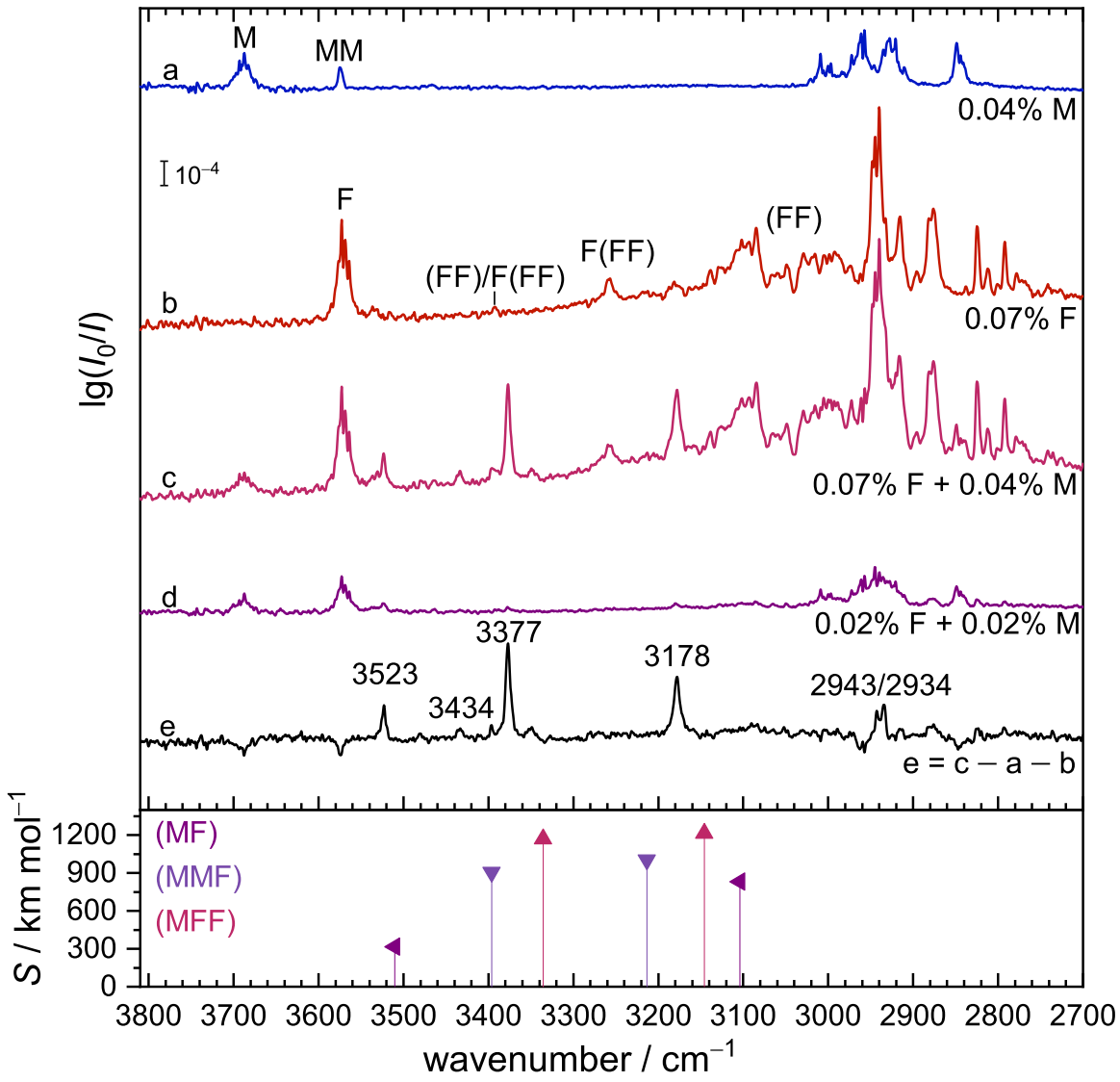

Fig. S3 *Filet* jet FTIR spectra of methanol in helium (a, 358 scans), formic acid in helium (b, 100 scans) and mixtures of both in helium with different concentrations of formic acid (c+d, 300/350 scans, d see also Figs. 2+3, high dilution), all at a stagnation pressure of 750 mbar. Trace e (see also Fig. 2f and 3f in the main text) shows the difference spectrum of trace c obtained by subtracting the unscaled single substance spectra from that of the mixture. The harmonically calculated (B3LYP-D3(BJ)/def2-QZVP), scaled (×0.96) band positions of the OH stretching vibrations of the global minimum structure of the mixed dimer (MF) and trimers (MMF) and (MFF) are shown below the experimental spectra.

S1.3 Sec. 3.4 "Auxiliary Raman spectra"

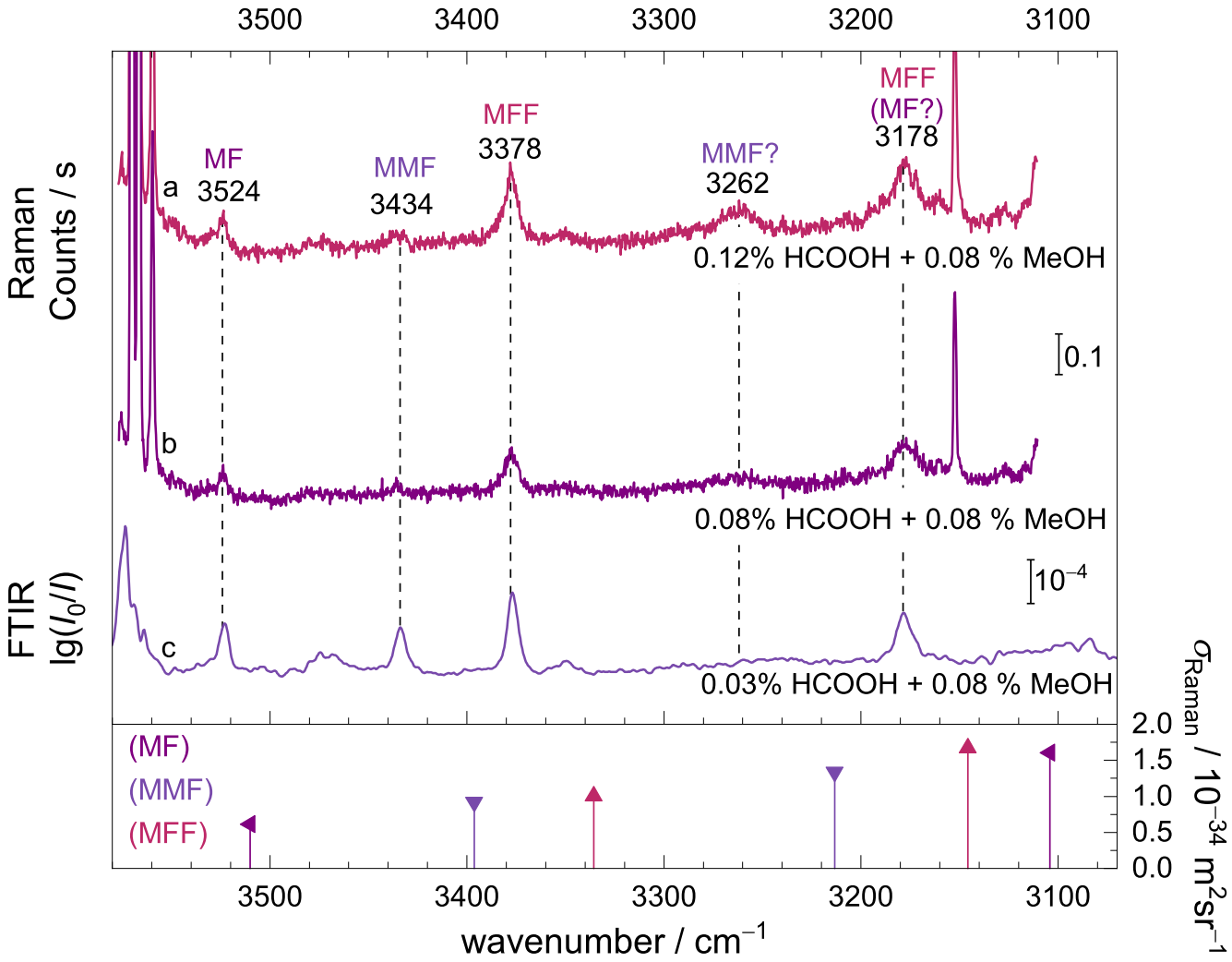

Fig. S4 OH stretching Raman (a, b) and FTIR (c, see also Figs. 2c+3c) spectra of the methanol and formic acid mixture expanded in helium with different concentrations. Each Raman spectrum is averaged over 6 data collections of 300 s duration. The band positions of the mixed clusters are included. The harmonically calculated (B3LYP-D3(BJ)/def2-QZVP), scaled (0.96) band positions of the OH stretching vibrations of the global minimum structure of the mixed dimer (MF), and trimers (MMF) and (MFF) are shown below the experimental spectra.

S1.4 Sec. 3.5 "What is different for OD stretching?"

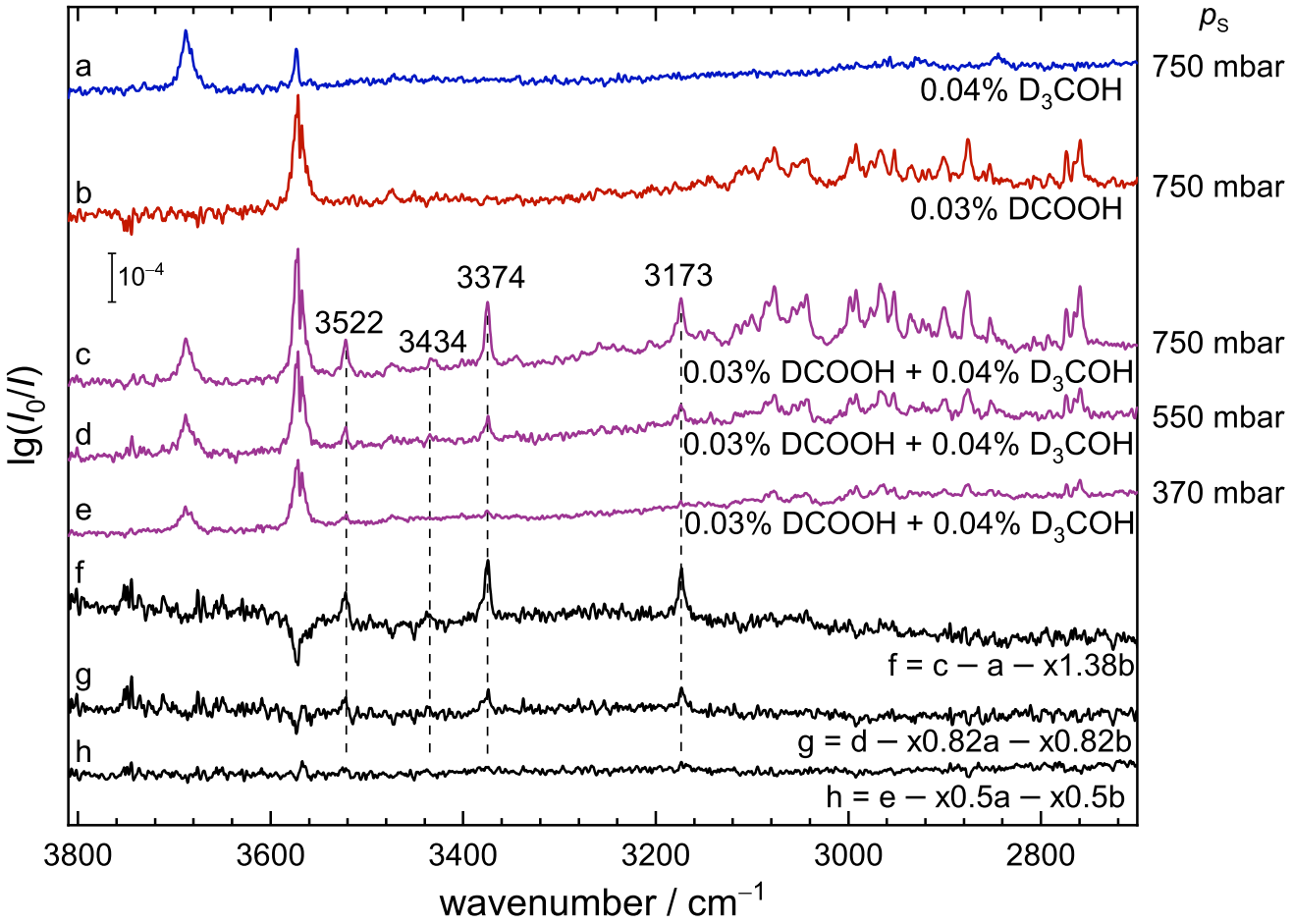

Fig. S5 *Filet* jet FTIR spectra of CD_3OH in helium (a, 200 scans), DCOOH in helium (b, 90 scans) and a mixture of both in helium at different stagnation pressures (c-e, 300/100/300 scans). Traces f-h show difference spectra of the mixtures corrected by scaled single substance spectra (for trace f see also the grey trace in Fig. 3). The scaling factors are displayed in the figure.

S1.5 Sec. 3.7 "Insights from and benchmarking of anharmonic (VPT2) calculations"

Tab. S9 Raw data (in cm^{-1}) visualised in Fig. 7 of the main text (calc − exp). "A" corresponds to scaled (×0.96) harmonic B3LYP-D3(BJ)/def2-QZVP wavenumbers whereas "B" and "C" are VPT2 wavenumbers from hybrid CCSD(T)-F12a/VDZ-F12//MP2/aVXZ force fields (B: X=D; C: X=T).

	Experiment	Calculation		
	IR	A	B	C
M	3685	3687	3673	3691
F	3570	3578	3563	3575
W	3756	3755	3753	3764
	3657	3657	3655	3668
MF	3523	3510	3506	3514
	3178[a]	3104	3085[b]	3087[c]
EM	3591	3562	3582	3592
EW		3731	3701[d]	3743[e]
	3587	3547	3574	3591
MMF	3434	3396	3420	3426
	3262[a]	3213	3217	3228
		2753		
MFF	3377	3336	3365	3369
	3178	3146	3192	3182
		2681		

[a] Hypothetical (MF) or tentative (MMF) experimental assignment (see main text for details).

[b] Fermi triad at **3085**, 3152, and 3193 (fundamental bolded).

[c] Different Fermi triad at **3087**, 3133, and 3175 (fundamental bolded).

[d] Fermi dyad at **3701** and 3719 (fundamental bolded).

[e] Fermi dyad at 3730 and **3743** (fundamental bolded).

S1.6 Sec. 3.9 "Ester detection by solvent vibrations"

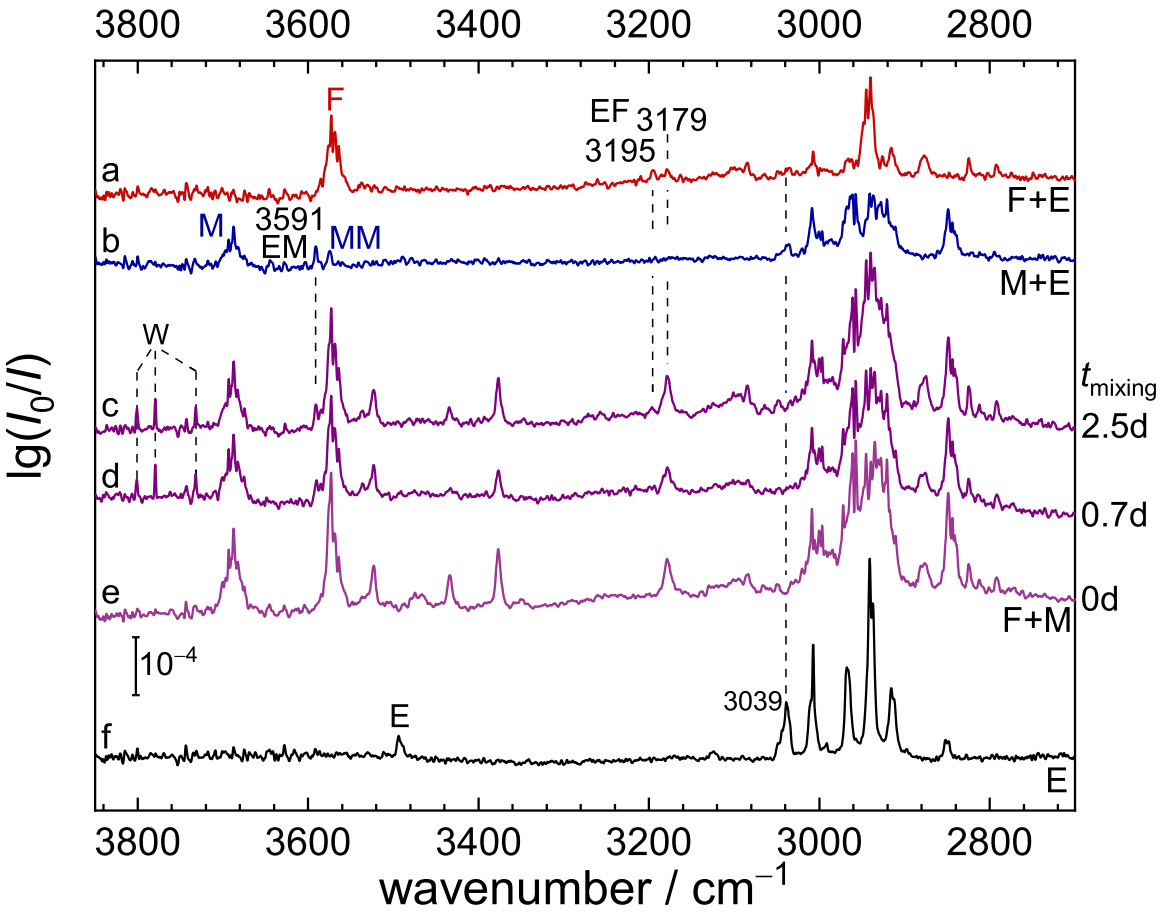

Fig. S6 Spectra of the premixed methanol and formic acid. Comparison of online mixing (trace e) with higher mixing times t_{mixing} of 0.7 and 2.5 days (trace d+c). In the main text the spectra are cut off at 3000 cm^{-1}. Note that the spectra c and d were obtained from two independent, nominally equal gas mixtures. Spectral variations can be due to variations in original mixing composition or due to the different storage time in the mixing bottle

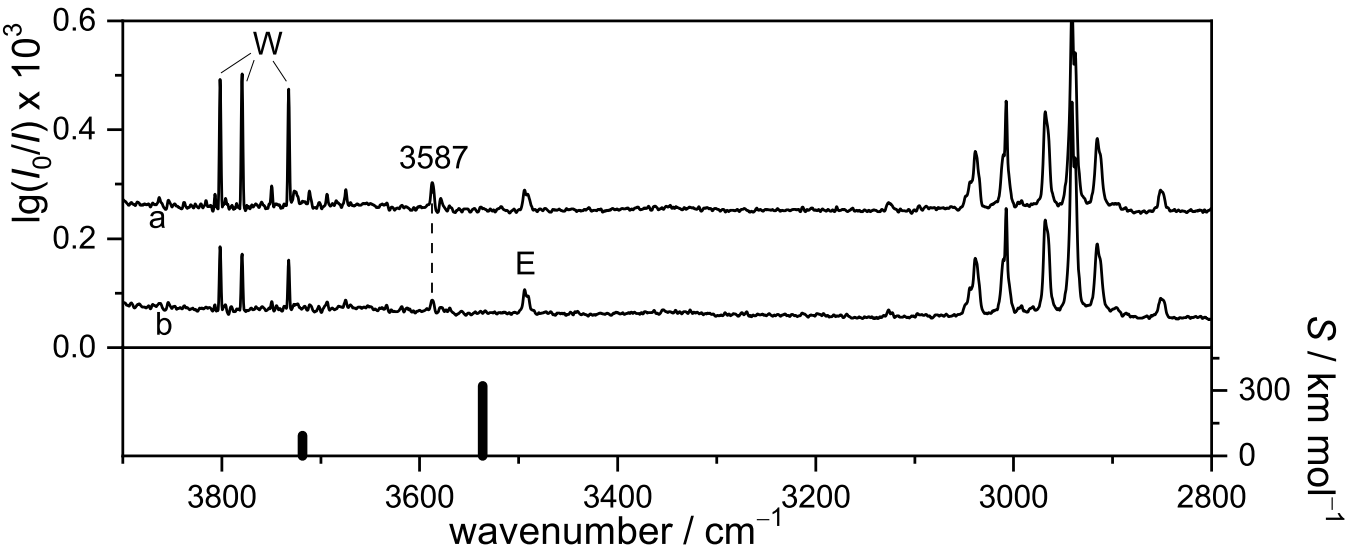

Fig. S7 FTIR spectra measured with the *gratin* jet (see Reference (*18*) for experimental details) of 0.04 % methyl formate (E) in helium at 750 mbar with increasing water concentrations (W) from b to a (each 400 scans). The scaled (×0.96) OH vibrations of EW at B3LYP-D3(BJ)/def2-QZVP level are shown at the bottom.

S2 Experimental details

Tab. S10 List of the purity and supplier of the used chemicals.

Chemical	Purity	Deuteration	Manufacturer
Methanol (M)	>99 %	-	abcr
	>99.99 %	-	Fischer science
Methanol (M)	99.9 % (99.8 % D-atom)	CD	euriso-top
Methanol (M)	(99.5 % D-atom)	OD	Merck
Formic acid (F)	98 %	-	Acros organics
	98 %	-	J&K
Formic acid (F)	95 % (98 % D-atom)	CD	abcr
Formic acid (F)	95 % (98 % D-atom)	OD	abcr
Methyl formate (E)	>99 %	-	Fluka
Water (W)		-	house water
Helium	≥99.996 %		Nippon Gas
	≥99.996 %		Linde

Tab. S11 Experimental details for the shown Raman jet spectra. Each spectrum was recorded with 2.0 bar helium pressure at the saturators, 0.7 bar reservoir pressure and the feeding lines at room temperature but with different nozzle temperatures (θ_n). The laser beam (532.274 nm) with the laser power P_L crossed the expansion with a distance of 1 mm to the nozzle. The monochromator was set at 647.2 nm and every spectrum is averaged over N_{Scan} scans with an exposure time of t_e. The saturator temperatures for formic acid (F, θ_F) and methanol (M, θ_T) are listed. For the generation of the gas mixture, gas flow meters were used (online mixing O). 'F (in He) : M (in He) : He' shows the individual flow meter settings for internal reference. For calibration and conversion to wavenumbers, atomic transitions of a neon discharge lamp were used. The date the spectra were recorded as well as the despike method (M_{des}) and the filename are listed for internal reference. All mixtures listed here were online mixed (see main text).

Figure, Trace	θ_F °C	θ_M °C	F (in He) : M (in He) : He	θ_n °C	t_e s	N_{Scan}	P_L W	M_{des}	Date YY:MM:DD	Filename
4a	10	−20	20 : 100 : 90	rt	600	3	20	led	21:04:19	20210419_g_FA_[...]_led_avg_cal.dat
4b	10	−20	10 : 100 : 100	rt	600	4	20	led	21:04:19	20210419_f_FA_[...]_led_avg_cal.dat
4c	10	−20	10 : 200 : 100	rt	600	3	20	led	21:04:19	20210419_h_FA_[...]_led_avg_cal.dat
4d[a]	10	−20	10 : 100 : 100	rt	600	4	20	led	21:04:19	20210419_f_FA_[...]_led_avg_cal.dat
	10	−20	10 : 100 : 100	30	600	4	20	led	21:04:22	20210422_a_FA_[...]_led_avg_cal.dat
4e	10	−20	10 : 100 : 100	50	600	3	20	des	21:04:19	20210422_b_FA_[...]_des_avg_cal.dat
4f[a]	10	−20	10 : 100 : 100	75	600	5	20	des	21:04:22	20210422_c_FA_[...]_des_avg_cal.dat
	10	−20	10 : 100 : 100	100	600	3	20	des	21:04:22	20210422_d_FA_[...]_des_avg_cal.dat
S4a	10	[b]	9 : 30[c] : 100	rt	300	6	25	des	20:01:21	200121_b_FA_[...]_des_cal.dat
S4b	10	[b]	6 : 30[c] : 100	rt	300	6	25	des	20:01:21	200121_a_FA_[...]_des_cal.dat

[a] The shown spectrum was averaged over these two spectra, [b] instead of the saturator a mixing bottle was used with 100 mbar in 50 bar helium (0.2 %), [c] a larger flow meter was used.

Tab. S12 Each IR spectrum was recorded with an aperture of 3.5 mm, an InSb/MCT sandwich detector, a spectral bandpass filter transparent between 2500 and 4100 cm^{-1} (internal reference: F13a), CaF_2 optics and a resolution of 2 cm^{-1}. The helium pressure in the gas pipes was at 1.6 bar and the reservoir pressure at 750 mbar. For each measurement, a mixed-gas bottle with defined concentrations was prepared, e.g. for 2c, 20 mbar formic acid (F) was prepared with 50 bar helium ($p_{He,\,mix}$) and mixed together 1:1 with a bottle of 40 mbar methanol (M) prepared in 25 bar helium ($p_{He,\,mix}$) which leads to a concentration (mole fraction) of 0.03 % F and 0.08 % M. 'F : M (: E)' shows the individual conditions while c(X) stands for the actual concentration (or mole fraction x) in the spectra, E stands for the ester methyl formate. The corresponding mixing methods online (O) or pre-mixing (P) are also listed under "Mixing". The spectra were averaged over multiple scans, with N_{Scan} as the amount of averaged scans. The date the spectra were recorded as well as the filename are listed for internal reference.

Figure, Trace	F : M (: E) / mbar	$p_{He,\,mix}$ / bar	c(F) : c(M) (:c(E)) / %	Mixing	N_{Scan}	Date / YY:MM:DD	Filename
2a+3a	10 : –	50	0.03 : –	O	375	19:08:19	190829-a-FA-[...].375.dpt
2b+3b	– : 40	50	– : 0.08	O	350	16:04:29	160429-a-MeOH_[..].350.dpt
2+3 h.d.+S3d	10 : 20	50 : 50	0.02 : 0.02	O	350	19:10:28	191028-f-FA-[..].350.dpt
2c+3c+5a	20 : 40	50 : 25	0.03 : 0.08	O	300	19:11:19	191119-b-MeOH-[..].300.dpt
2f+3f					see S3e		
3 C-D					see S5f		
5b[a]	10 : 40	25 : 25	0.03 : 0.08	O	350	23:07:05	20230705-a-d-MeOD-[..].350.dpt
9a+S6a	10 : – (: 10)	50 : 50	0.03 : – (: 0.02)	O	300	19:10:28	191028-g-FA-[...].300.dpt
9b+S6b	– : 20 (: 10)	50 : 50	– : 0.04 (: 0.02)	O	350	19:11:04	191104-a-MeOH-[...].350.dpt
9c+S6c	10 : 20	50	0.02 : 0.04	P	350	19:12:09	191209-a-MeOH-[...]].350.dpt
9d+S6d	10 : 20	50	0.02 : 0.04	P	365	19:10:17	191017-a-FA-[...]365.dpt
9e[b]+S6e[b]	10 : 20	50 : 50	0.02 : 0.02	O	350	19:10:28	191028-f-FA-[...].350.dpt
	20 : 40	50 : 25	0.02 : 0.08	O	300	19:11:19	191119-b-MeOH-[...].300.dpt
9f+S6f	– : – (: 20)	50	– : – : 0.04	O	405	19:11:06	191106-a-MF-[...].405.dpt
S3a	– : 20	50	– : 0.04	O	358	19:10:22	191022-a-MeOH-[...].358.dpt
S3b	38.2 : –	50	0.07 : – (He)	O	100	20:01:30	200130-m+n-FA-[...].100.dpt
S3c	38.2 : 40	50 : 50	0.07 : 0.04	O	300	20:01:30	200130-a-f-FA-[...].300.dpt
S5a	– : 40	50	– (He) : 0.04	O	200	20:02:12	200212-n-dMeOH-[...].200.dpt
S5b	20 : –	50	0.03 : – (He)	O	90	20:02:12	200212-m-FdA-[...].90.dpt
S5c[c]	20 : 40	50:50	0.03 : 0.04	O	300	20:02:12	200212-b-e-FdA-[...].300.dpt
S5d[d]	20 : 40	50:50	0.03 : 0.04	O	300	20:02:12	200212-b-e-FdA-[...].300.dpt
S5e	20 : 40	50:50	0.03 : 0.04	O	300	20:02:12	200212-b-e-FdA-[...].300.dpt
S7a[e]			– : – (: 0.04)		400	19:11:25	20191125-defg-Methylformiat-[...].400.dpt
S7b[e]			– : – (: 0.04)		400	19:11:20	20191120-efgh-Methylformiat-[...].400.dpt

[a] A different filter F21 (4600-600 cm^{-1}) was used with the slightly different InSb2mmII detector and 2.5 mm aperture, [b] the shown spectrum was averaged over these two spectra, [c] 550 mbar reservoir pressure instead of 750 mbar, [d] 370 mbar reservoir pressure instead of 750 mbar, [e] a different FTIR setup was used with 0.04 % of E in helium, see Reference (*18*) for experimental details.

S2.1 Details for the concentration calculations of the IR spectra

For convenience, the calculation for the concentrations (expressed as mole fractions x) for a gas mixture is exemplified for Figure 2, trace c. The corresponding mixing conditions for this and the other spectra can be found in Tab. S12.
For methanol 40 mbar were filled into an empty gas bottle at room temperature, which was then filled up to 25 bar with helium. The fraction $x(\mathrm{M})$ is estimated via its vapor pressure $p(\mathrm{M})$ in relation to the total pressure p_{total} under the assumption of ideal behavior:

$$x_{\text{gas bottle 1}}(\mathrm{M}) \approx \frac{p(\mathrm{M})}{p_{\mathrm{total}}} = \frac{40 \cdot 10^{-3}\ \mathrm{bar}}{25\ \mathrm{bar}} = 0.16\ \% \tag{S2}$$

For formic acid 20 mbar were used in a second empty gas bottle, which was then filled up to 50 bar with helium. Because formic acid has a pronounced tendency to form dimers at room temperature with a K_{p} around 300[19,20], this has to be taken into account for a more accurate estimation of the concentration. The measured vapor pressure p_{vapor} of 20 mbar ($= 20 \cdot 10^2$ Pa) is the sum of the monomer p_{monomer} and dimer pressure p_{dimer} (Eq. S3). The partial pressure p_i, which will be used for the calculation of the formic acid fraction (similar to S2), is then the sum of the monomer p_{monomer} and two times the dimer pressure p_{dimer} (Eq. S4). This Equation S4 was obtained by solving the law of mass action, Equation S5, for p_{monomer} and using a standard pressure of $p_0 = 10^5$ Pa.

$$p_{\mathrm{vapor}} = p_{\mathrm{monomer}} + p_{\mathrm{dimer}} \tag{S3}$$

$$\begin{aligned} p_i &= \left(\underbrace{-\frac{p_0}{2K_{\mathrm{p}}} + \sqrt{\left(\frac{p_0}{2K_{\mathrm{p}}}\right)^2 + \frac{p_{\mathrm{vapor}}\, p_0}{K_{\mathrm{p}}}}}_{p_{\mathrm{monomer}}} \right) + 2 \cdot \underbrace{(p_{\mathrm{vapor}} - p_{\mathrm{monomer}})}_{p_{\mathrm{dimer}}} \\ &= \left(\underbrace{-\frac{10^5\ \mathrm{Pa}}{2 \cdot 300} + \sqrt{\left(\frac{10^5\ \mathrm{Pa}}{2 \cdot 300}\right)^2 + \frac{20 \cdot 10^2\ \mathrm{Pa} \cdot 10^5\ \mathrm{Pa}}{300}}}_{p_{\mathrm{monomer}}} \right) + 2 \cdot (20 \cdot 10^2\ \mathrm{Pa} - p_{\mathrm{monomer}}) \\ &= 3333.3\ \mathrm{Pa} \approx 33.3\ \mathrm{mbar} \end{aligned} \tag{S4}$$

$$K_{\mathrm{p}} = \frac{p_{\mathrm{dimer}} \cdot p_0}{p_{\mathrm{monomer}}^2} \tag{S5}$$

$$x_{\text{gas bottle 2}}(\mathrm{F}) \approx \frac{p_i(\mathrm{F})}{p_{\mathrm{total}}} = \frac{33.3 \cdot 10^{-3}\ \mathrm{bar}}{50\ \mathrm{bar}} = 0.067\ \% \tag{S6}$$

To finalise the actual mole fraction in the mixture for method O, it must be taken into account that both prepared gas mixtures were mixed 1:1 at the same pressure to create the actual measured mixture, which leads to a dilution by the factor of 2 for both the methanol and formic acid concentration:

$$\begin{aligned} x(\mathrm{M}) &= x_{\text{gas bottle 1}}(\mathrm{M})/2 \approx 0.08\ \% \\ x(\mathrm{F}) &= x_{\text{gas bottle 2}}(\mathrm{F})/2 \approx 0.03\ \% \end{aligned} \tag{S7}$$

References

1. S. Grimme, J. Antony, S. Ehrlich, H. Krieg, *J. Chem. Phys.* **132**, 154104 (2010).
2. S. Grimme, S. Ehrlich, L. Goerigk, *J. Comput. Chem.* **32**, 1456–1465 (2011).
3. F. Weigend, *Phys. Chem. Chem. Phys.* **4**, 4285–4291 (2002).
4. *TURBOMOLE V7.5 2020, a development of University of Karlsruhe and Forschungszentrum Karlsruhe GmbH, 1989-2007, TURBOMOLE GmbH, since 2007; available from https://www.turbomole.org.*
5. T. B. Adler, G. Knizia, H.-J. Werner, *J. Chem. Phys.* **127**, 221106 (2007).
6. W. Győrffy, G. Knizia, H.-J. Werner, *J. Chem. Phys.* **147**, 214101 (2017).
7. H.-J. Werner, P. J. Knowles, G. Knizia, F. R. Manby, M. Schütz, *WIREs Comput Mol Sci* **2**, 242–253 (2011).
8. H.-J. Werner *et al.*, *J. Chem. Phys.* **152**, 144107 (2020).
9. H.-J. Werner *et al.*, *MOLPRO, version 2022.1, a package of ab initio programs*, see https://www.molpro.net, Stuttgart, Germany.
10. R. A. Bachorz *et al.*, *J. Comput. Chem.* **32**, 2492–2513 (2011).
11. C. Hättig, D. P. Tew, A. Köhn, *J. Chem. Phys.* **132**, 231102 (2010).
12. O. Marchetti, H.-J. Werner, *Phys. Chem. Chem. Phys.* **10**, 3400 (2008).
13. S. Grimme, *J. Chem. Theory Comput.* **15**, 2847–2862 (2019).
14. S. Grimme, C. Bannwarth, P. Shushkov, *J. Chem. Theory Comput.* **13**, 1989–2009 (2017).
15. C. Bannwarth, S. Ehlert, S. Grimme, *J. Chem. Theory Comput.* **15**, 1652–1671 (2019).
16. P. Pracht, E. Caldeweyher, S. Ehlert, S. Grimme, *ChemRxiv* (2019, 10.26434/chemrxiv.8326202.v1).
17. *Origin(Pro) OriginLab Corporation, Northampton, MA, USA*. Version 2022.
18. H. C. Gottschalk *et al.*, *Instruments* **5**, 12 (Mar. 2021).
19. J. V. Auwera, K. Didriche, A. Perrin, F. Keller, *J. Chem. Phys.* **126**, 124311 (Mar. 2007).
20. K. Mackeprang, Z.-H. Xu, Z. Maroun, M. Meuwly, H. G. Kjaergaard, *Phys. Chem. Chem. Phys.* **18**, 24654–24662 (2016).